Anal. Chem. 2010, 82, 8095–8105

Mass Spectrometry-Based Fragmentation as an Identification Tool in Lignomics

Kris Morreel,*,†,‡ Hoon Kim,§ Fachuang Lu,§ Oana Dima,†,‡ Takuya Akiyama,|| Ruben Vanholme,†,‡ Claudiu Niculaes,†,‡ Geert Goeminne,†,‡ Dirk Inzé,†,‡ Eric Messens,†,‡ John Ralph,§ and Wout Boerjan*,†,‡

Department of Plant Systems Biology, VIB, B-9052 Ghent, Belgium, Department of Plant Biotechnology and Genetics, Ghent University, B-9052 Ghent, Belgium, Department of Biochemistry and DOE Great Lakes Bioenergy Research Center, University of Wisconsin, Madison, Wisconsin 53706, and Department of Biomaterial Sciences, Graduate School of Agricultural and Life Sciences, The University of Tokyo, Tokyo 113-8657, Japan

The ensemble of all phenolics for which the biosynthesis is coregulated with lignin biosynthesis, i.e., metabolites from the general phenylpropanoid, monolignol, and (neo)-lignan biosynthetic pathways and their derivatives, as well as the lignin oligomers, is coined the lignome. In lignifying tissues, the lignome comprises a significant portion of the metabolome. However, as is true for metabolomics in general, the structural elucidation of unknowns represents the biggest challenge in characterizing the lignome. To minimize the necessity to purify unknowns for NMR analysis, it would be desirable to be able to extract structural information from liquid chromatography−mass spectrometry data directly. However, mass spectral libraries for metabolomics are scarce, and no libraries exist for the lignome. Therefore, elucidating the gas-phase fragmentation behavior of the major bonding types encountered in lignome-associated molecules would considerably advance the systematic characterization of the lignome. By comparative MS^n analysis of a series of molecules belonging to the *β*-aryl ether, benzodioxane, phenylcoumaran, and resinol groups, we succeeded in annotating typical fragmentations for each of these bonding structures as well as fragmentations that enabled the identification of the aromatic units involved in each bonding structure. Consequently, this work lays the foundation for a detailed characterization of the lignome in different plant species, mutants, and transgenics and for the MS-based sequencing of lignin oligomers and (neo)lignans.

Lignin is an aromatic heteropolymer that is mainly present in secondary-thickened plant cell walls where it provides the necessary strength and hydrophobicity for plants to grow in an upward direction and to enable the transport of water, nutrients, and photoassimilates. Lignin is mainly composed of *p*-hydroxyphenyl (**H**), guaiacyl (**G**), and syringyl (**S**) units derived from the combinatorial coupling of *p*-coumaryl, coniferyl, and sinapyl alcohols (Figure 1A),[1] the so-called monolignols that are produced by the general phenylpropanoid and monolignol biosynthetic pathways.[2−5] Following oxidation by peroxidase and/or laccase, the resulting electron-delocalized monolignol radical has unpaired electron density at its 1-, 3-, O-4-, 5-, and 8-positions (Figure 1B). As radical coupling at the 8-position is favored, coupling with another monolignol radical results in, after rearomatization, a mixture of dehydrodimers with 8−8′, 8−5′, and 8−O-4′ linkages (Figure 1C).

In addition to these major monomers, several other monomers have been identified in particular species or in plants with modified lignin biosynthesis,[1,3] such as 5-hydroxyconiferyl alcohol in caffeic acid *O*-methyltransferase (COMT) downregulated transgenic plants,[6,7] dihydroconiferyl alcohol in cinnamyl alcohol dehydrogenase (CAD) deficient loblolly pine,[8] acylated monolignols, such as sinapyl *p*-hydroxybenzoate in poplar,[9] and hydroxycinnamic acid or hydroxycinnamate esters, such as feruloyl tyramine in tobacco.[10,11] As a result of the combinatorial complexity of radical coupling reactions and the variety of monomers, the number of possible dimers is quite large. In addition to dimers, incipient lignification yields a variety of small lignin oligomers in lignifying

* To whom correspondence should be addressed. E-mail: kris.morreel@psb.vib-ugent.be (K.M.) and wout.boerjan@psb.vib-ugent.be (W.B.).

† VIB.

‡ Ghent University.

§ University of Wisconsin.

|| The University of Tokyo.

(1) Ralph, S. A.; Landucci, L. L.; Ralph, J. NMR Database of Lignin and Cell Wall Model Compounds. 2004 (http://ars.usda.gov/Services/docs.htm?docid=10491).

(2) Boerjan, W.; Ralph, J.; Baucher, M. *Annu. Rev. Plant Biol.* **2003**, *54*, 519–546.

(3) Vanholme, R.; Morreel, K.; Ralph, J.; Boerjan, W. *Curr. Opin. Plant Biol.* **2008**, *11*, 278–285.

(4) Vanholme, R.; Demedts, B.; Morreel, K.; Ralph, J.; Boerjan, W. *Plant Physiol.* **2010**, *153*, 895–905.

(5) Vanholme, R.; Van Acker, R.; Boerjan, W. *Trends Biotechnol.* **2010**, in press.

(6) Ralph, J.; Lapierre, C.; Lu, F.; Marita, J. M.; Pilate, G.; Van Doorsselaere, J.; Boerjan, W.; Jouanin, L. *J. Agric. Food Chem.* **2001**, *49*, 86–91.

(7) Morreel, K.; Ralph, J.; Kim, H.; Lu, F.; Goeminne, G.; Ralph, S.; Messens, E.; Boerjan, W. *Plant Physiol.* **2004**, *136*, 3537–3549.

(8) Ralph, J.; MacKay, J. J.; Hatfield, R. D.; O'Malley, D. M.; Whetten, R. W.; Sederoff, R. R. *Science* **1997**, *277*, 235–239.

(9) Morreel, K.; Ralph, J.; Lu, F.; Goeminne, G.; Busson, R.; Herdewijn, P.; Goeman, J. L.; Van der Eycken, J.; Boerjan, W.; Messens, E. *Plant Physiol.* **2004**, *136*, 4023–4036.

(10) Ralph, J.; Garcia Conesa, M. T.; Williamson, G. *J. Agric. Food Chem.* **1998**, *46*, 2531–2532.

(11) Dauwe, R.; Morreel, K.; Goeminne, G.; Gielen, B.; Rohde, A.; Van Beeumen, J.; Ralph, J.; Boudet, A.-M.; Kopka, J.; Rochange, S. F.; Halpin, C.; Messens, E.; Boerjan, W. *Plant J.* **2007**, *52*, 263–285.

10.1021/ac100968g
Published on Web 08/26/2010

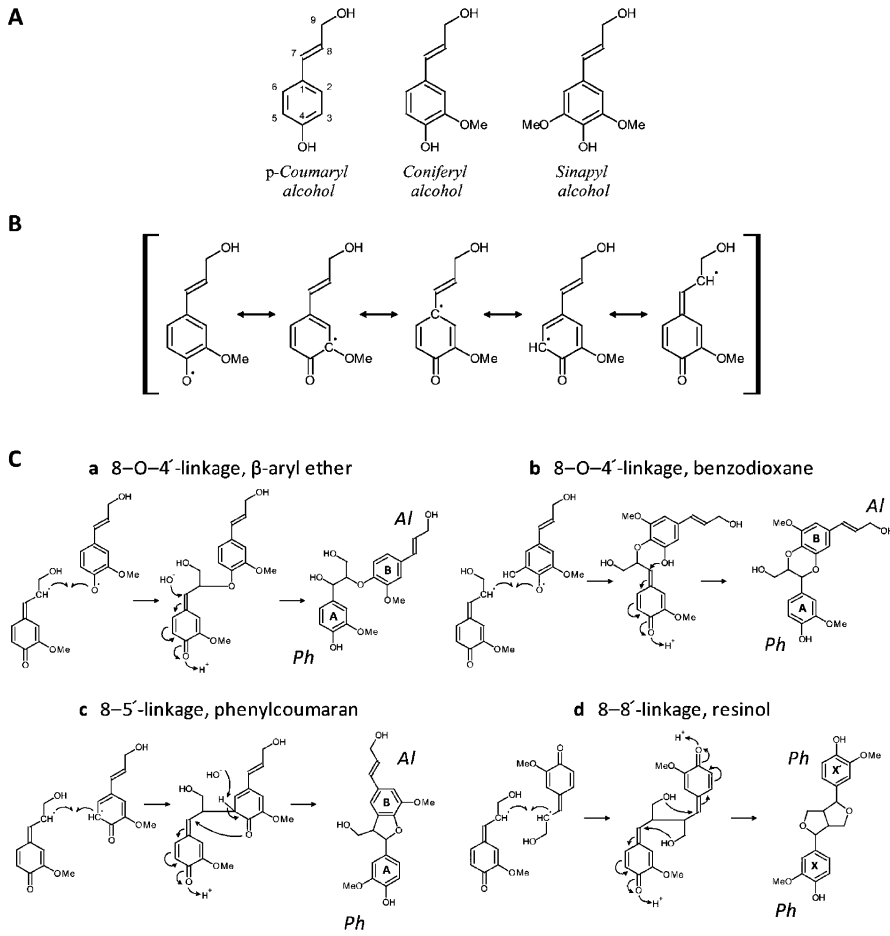

Figure 1. Radical−radical dimerization of monolignols. (A) Monolignols. (B) Radical delocalization following monolignol oxidation, illustrated for the coniferyl alcohol radical. (C) Main monolignol (dehydro)dimerization reactions: *Ph*, phenolic end group; *Al*, aliphatic end group. For all compounds except the resinols, the phenolic and aliphatic end groups correspond to the A and B rings, respectively. Resinols contain two phenolic end groups corresponding to the X and X′ rings.

tissues. Furthermore, the monolignols also serve for the production of lignans and neolignans. Both compound classes are secondary metabolites for which the biosynthesis starts with the radical−radical coupling of monolignols, possibly directed by dirigent proteins, providing the same dehydrodimers with the same linkages that are observed in lignin. Whereas lignification is racemic, producing non-optically active dehydrodimers and higher-order oligomers, the dimerization in lignan biosynthesis is, however, stereospecifically controlled. Further enzymatic conversions lead to a plethora of more complex lignans.

When lignifying plant tissues (such as xylem) are profiled, with reversed-phase liquid chromatography−mass spectrometry (LC−MS), most of the peaks are associated with lignin biosynthesis. Hence, their abundances are coregulated and have been shown to change in transgenic plants in which lignin biosynthesis has been misregulated.[9,11−15] The identification of these compounds has contributed significantly to our understanding of phenylpropanoid and lignin biosynthesis. To gain a more complete view of the consequences of lignin pathway perturbations and to identify novel biosynthetic routes, the identity of a maximum number of these compounds must be resolved.[5] We coin the term "lignome" to describe the full suite of these lignin-associated phenolics, and their profiling and identification as "lignomics". Although the lignome constitutes a major fraction of the metabolome of lignifying tissues,[7,11,14,15] efficient metabolomics tools for lignomics are not yet available. In metabolomics, multiple methods are often combined to profile as many metabolites as possible because of the varying physicochemical properties of these small molecules.[16] Generally, gas chromatography−mass spectrometry (GC−MS) and/or LC−MS is used. Whichever method is applied, only a minority of the peaks represent known compounds.[17] Although this drawback has been mentioned repetitively in the metabolomics community, hardly any significant effort has been

(12) Meyermans, H.; Morreel, K.; Lapierre, C.; Pollet, B.; De Bruyn, A.; Busson, R.; Herdewijn, P.; Devreese, B.; Van Beeumen, J.; Marita, J. M.; Ralph, J.; Chen, C.; Burggraeve, B.; Van Montagu, M.; Messens, E.; Boerjan, W. *J. Biol. Chem.* **2000**, *275*, 36899–36909.
(13) Rohde, A.; Morreel, K.; Ralph, J.; De Rycke, R.; Kushnir, S.; Van Doorsselaere, J.; Goeminne, G.; Joseleau, J.-P.; Vuylsteke, M.; Van Driessche, G.; Van Beeumen, J.; Messens, E.; Boerjan, W. *Plant Cell* **2004**, *16*, 2749–2771.
(14) Damiani, I.; Morreel, K.; Danoun, S.; Goeminne, G.; Yahiaoui, N.; Marque, C.; Kopka, J.; Messens, E.; Goffner, D.; Boerjan, W.; Boudet, A. M.; Rochange, S. F. *Plant Mol. Biol.* **2005**, *59*, 753–769.
(15) Leplé, J.-C.; Dauwe, R.; Morreel, K.; Storme, V.; Lapierre, C.; Pollet, B.; Naumann, A.; Kang, K.-Y.; Kim, H.; Ruel, K.; Lefèbvre, A.; Joseleau, J.-P.; Grima-Pettenati, J.; De Rycke, R.; Andersson-Gunneråas, S.; Erban, A.; Fehrle, I.; Petit-Conil, M.; Kopka, J.; Polle, A.; Messens, E.; Sundberg, B.; Mansfield, S.; Ralph, J.; Pilate, G.; Boerjan, W. *Plant Cell* **2007**, *19*, 3669–3691.
(16) Dettmer, K.; Aronov, P. A.; Hammock, B. D. *Mass Spectrom. Rev.* **2007**, *26*, 51–78.
(17) Schauer, N.; Steinhauser, D.; Strelkov, S.; Schomburg, D.; Allison, G.; Moritz, T.; Lundgren, K.; Roessner-Tunali, U.; Forbes, M. G.; Willmitzer, L.; Fernie, A. R.; Kopka, J. *FEBS Lett.* **2005**, *579*, 1332–1337.

initiated to systematically unravel the structures of the unknown compounds in a metabolite profile, because often laborious purifications are involved to identify unambiguously the compound by NMR.

Complementary to NMR, MS affords information about the structure of a given compound, but correct interpreting MS fragmentation spectra necessitates knowledge of the dissociation pathways in the gas phase. In GC−MS, radical cations that are generated by the loss of an electron in the electron impact (EI) ionization source[18] fragment in-source according to well-studied pathways. Because of the reproducibility of the EI ionization method, libraries containing hundreds of thousands of EI-MS spectra, e.g., Wiley or NIST, have been created. However, GC enables the profiling of only the low-molecular mass lignome-associated molecules, yet a more comprehensive profiling can be obtained using LC. In LC−MS, soft ionization is applied to allow the evaporation of the mobile phase. Here, a proton is attached to (positive-ion mode) or abstracted from (negative-ion mode) the molecule, providing a pseudomolecular parent ion that fragments little in the ionization source. In the case of phenolics, the negative-ion mode is often preferred because it is more sensitive than the positive-ion mode. Fragmentation of the pseudomolecular parent ion is mainly evoked in the analyzer by collision-induced dissociation (CID). Consequently, the resulting MS/MS ("in-space" CID) or MS^n ("in-time" CID) spectrum is influenced by the type of ionization source, the source settings, the analyzer, the collision gas, and the collision energy. The latter parameter is thought to be less important in MS^n.[19,20] This dependence on several parameters has severely impeded the creation of MS/MS or MS^n libraries. Furthermore, although pseudomolecular cations obey even-electron fragmentation rules, the dissociation of pseudomolecular anions can occur either via heterolytic or via homolytic cleavages and might involve ion−neutral complexes. Last but not least, charge-remote fragmentations are more prevalent than in positive ionization mode.[21] Consequently, research aimed at the CID pathways of anions is almost lacking for all secondary metabolites except the flavonoids.[22,23]

Here, the negative-ion gas-phase fragmentation pathways of the major bonding structures that are encountered in the lignome, i.e., in the 8−O-4′ linkage-associated β-aryl ethers and benzodioxanes, the 8−5′ linkage-associated phenylcoumarans, and the 8−8′ linkage-associated resinols, are investigated by analyzing MS^n spectra of a series of dimers. Although both charge-driven, i.e., fragmentations that start from the most acidic site,[24] and charge-remote reactions might be responsible for the fragmentations, the former type will occur whenever possible;[25] a charge-remote fragmentation is only considered when no charge-driven pathway is possible. The resolved fragmentation pathways will enable a more efficient structural elucidation of unknowns present in the lignome and, additionally, provide a framework for the construction of a MS-based sequencing strategy for lignin oligomers[26] and (neo)lignans containing more than two phenylpropane units, called the sesquineolignans and the dilignans, for which no sequencing methods are yet available.

Table 1. Shorthand Names for Lignin Oligomer Units[a]

Shorthand name	Unit type
H	*p*-Hydroxyphenyl, unit derived from *p*-coumaryl alcohol
G	Guaiacyl, unit derived from coniferyl alcohol
S	Syringyl, unit derived from sinapyl alcohol
FA	Unit derived from ferulic acid
G′	Unit derived from coniferaldehyde
S′	Unit derived from sinapaldehyde
5H	5-Hydroxyguaiacyl, unit derived from 5-hydroxyconiferyl alcohol
5H′	Unit derived from 5-hydroxyconiferaldehyde

[a] Structures of the monomers are shown in Figure 12 of the Supporting Information.

EXPERIMENTAL SECTION

Shorthand Naming of Oligolignols. The oligolignols were named as described previously.[7] The linkage type, i.e., 8−O-4′, 8−8′, and 8−5′, is indicated as (8−O-4), (8−8), and (8−5), respectively. Isomers (*threo* and *erythro*) of a β-aryl ether are indicated in parentheses as *t* and *e*, respectively. Units (**G**, **S**, **5H**, etc.) are written in bold outside the parentheses (Table 1).

Chemicals and Syntheses. All chemicals and synthesis reactions are described in the Experimental Section of the Supporting Information.

Direct Infusion MS^n Analysis of Standards. A 100 μM solution of each standard, flowing at a rate of 10 μL/min, was mixed with a flow of 300 μL/min (water/methanol, 50:50 (v:v), 0.1% acetate) before entering a LCQ Classic ion trap MS instrument (IT-MS) upgraded to a LCQ Deca instrument (Thermo Fisher Scientific, Waltham, MA). Analytes were negatively ionized by atmospheric pressure chemical ionization (APCI) using the following parameter values: source current, 5 μA; capillary temperature, 150 °C; vaporizer temperature, 350 °C; sheath gas, 25 arbitrary units; and auxiliary gas, 3 arbitrary units. MS^n analysis was performed by CID using He as the collision gas. The MS^n spectra were analyzed with Xcalibur version 1.2.

Whenever necessary, accurate MS data were obtained using Fourier Transform-Ion Cyclotron Resonance-MS (FT-ICR-MS; LTQ FT Ultra, Thermo Electron Corp., Bremen, Germany) with electrospray ionization (ESI) in the negative mode using the following parameter values: source voltage, 3.5 kV; capillary temperature, 300 °C; sheath gas, 30 arbitrary units. The standard was infused with a flow rate of 10 μL/min (water/methanol, 50:

(18) McLafferty, F. W.; Tureček, F. *Interpretation of Mass Spectra*, 4th ed.; University Science Books: Mill Valley, CA, 1993.
(19) Volná, K.; Holčapek, M.; Kolářová, L.; Lemr, K.; Čáslavský, J.; Kačer, P.; Poustka, J.; Hubálek, M. *Rapid Commun. Mass Spectrom.* **2008**, *22*, 101–108.
(20) Werner, E.; Heilier, J.-F.; Ducruix, C.; Ezan, E.; Junot, C.; Tabet, J.-C. *J. Chromatrogr., B* **2008**, *871*, 143–163.
(21) Bowie, J. H. *Mass Spectrom. Rev.* **1990**, *9*, 349–379.
(22) de Rijke, E.; Out, P.; Niessen, W. M. A.; Ariese, F.; Gooijer, C.; Brinkman, U. A. T. *J. Chromatogr., A* **2006**, *1112*, 31–63.
(23) Morreel, K.; Goeminne, G.; Storme, V.; Sterck, L.; Ralph, J.; Coppieters, W.; Breyne, P.; Steenackers, M.; Georges, M.; Messens, E.; Boerjan, W. *Plant J.* **2006**, *47*, 224–237.
(24) Thevis, M.; Schänzer, W.; Schmickler, H. *J. Am. Soc. Mass Spectrom.* **2003**, *14*, 658–670.
(25) Cheng, C.; Gross, M. L. *Mass Spectrom. Rev.* **2000**, *19*, 398–420.
(26) Morreel, K.; Dima, O.; Kim, H.; Lu, F.; Niculaes, C.; Vanholme, R.; Dauwe, R.; Goeminne, G.; Inzé, D.; Messens, E.; Ralph, J.; Boerjan, W. *Plant Physiol.* **2010**, *153*, 1464–1478.

50 (v:v), 0.1% acetate). MS^2 analysis was performed in the ion trap using a 5, 10, 15, 20, 25, 30, 35, or 40% collision energy and He as the collision gas. Accurate masses for the first product ions were obtained in the ion cyclotron using full scans between m/z 100 and 500. Whenever necessary, second product ions were generated using infrared multiphoton dissociation (IRMPD) with an 80% energy for 300 ms.

LC−MS Analysis. Operating conditions are described in the Experimental Section of the Supporting Information.

RESULTS AND DISCUSSION

***β*-Aryl Ethers and Benzodioxanes Are 8−O-4′-Linked Dimers.** The 8−O-4′ bonds (Figure 1Ca,b) arise when the 8-position of a monolignol radical couples with the O-4′-position of another monolignol radical. Rearomatization of the quinone methide intermediate involves an external nucleophile (usually water), and a so-called β-aryl ether bonding structure is formed (Figure 1Ca). However, if caffeyl or 5-hydroxyconiferyl alcohol is coupled via the O-4′-position, the 3′-OH or 5′-OH function internally traps the quinone methide, affording a benzodioxane structure (Figure 1Cb). Although benzodioxanes are present in minor amounts in lignin, they were shown to contribute substantially to the lignin of transgenic plants in which the level of 5-hydroxylation was increased and/or methylation of the 5-OH group was downregulated.[3,6,9]

MS^2 Spectra of *β*-Aryl Ethers. As shown in Table 2A, the MS^2 spectra of the monolignol-derived β-aryl ether dimers show small neutral losses of 18 Da (H_2O), 30 Da (CH_2O, formaldehyde), and 48 Da (H_2O/CH_2O), leading to the $[\underline{M - H^+} - H_2O]^-$, $[\underline{M - H^+} - CH_2O]^-$, and $[\underline{M - H^+} - H_2O - CH_2O]^-$ first product ions, with the peak from the latter often being the base peak. In addition, cleavage of the bonding structure provides the A^-, B^-, and $[A - CH_2O]^-$ first product ions, where A and B are moieties from the phenolic and aliphatic end groups, respectively. MS^n spectra of the first product ions and their accurate masses are shown in Figure 1 of the Supporting Information and Table 3, respectively. Additionally, their peak intensities relative to the applied collision energy in IT-MS or in quadrupole-time-of-flight MS (Q-Tof-MS) are displayed in Figure 11 of the Supporting Information. A summary of all fragmentation reactions is shown in Figure 2A, whereas a more detailed view is provided in Figure 2 of the Supporting Information. We suggest the reader to use the more detailed Supporting Information figures when reading the text. For the sake of convenience, throughout the text and figures (Figures 1, 2, and 5−10 of the Supporting Information), fragmentation pathway intermediates are denoted by the letter **i** followed by a unique number in boldface.

(i) $[\underline{M - H^+} - H_2O]^-$ First Product Ion. The water elimination can only come from the aliphatic alcohol groups. Following a charge-driven mechanism (Figure 2A of the Supporting Information), the 7-hydroxy function is expelled when the phenoxide anion **i1** is converted to a quinone methide. The hydroxide anion will then abstract an acidic proton from the quinone methide via an anion−neutral complex, yielding the first product ion **i2** (Figure 2A of the Supporting Information). Further support for the elimination of the 7-hydroxy function was obtained from MS^2 data of the model compounds shown in panels A−C of Figure 3 of the Supporting Information, in which the hydroxyl group is present at the 9-, 8-, and 7-positions, respectively. Whereas water loss yielded the base peak in the MS^2 spectrum of the latter compound, hardly any water loss was observed upon CID of the former two compounds.

(ii) $[\underline{M - H^+} - CH_2O]^-$ First Product Ion. Formaldehyde loss originates from the aliphatic alcohol functions (see also results and discussion of the Supporting Information), but a charge-driven process is difficult to deduce. Therefore, a charge-remote fragmentation mechanism[27] in which ions **i3** and **i4** might both contribute to the intensity of the $[\underline{M - H^+} - CH_2O]^-$ first product ion might be postulated (Figure 2B of the Supporting Information).

(iii) $[\underline{M - H^+} - H_2O - CH_2O]^-$ First Product Ion. The combined elimination of water and formaldehyde (−48 Da) proceeds by a charge-mediated stepwise or concerted reaction (Figure 2C of the Supporting Information). According to a stepwise reaction, the 9-alkoxide anion **i2** is subjected to a 1,2-elimination causing the fragmentation of the 8−9 bond and releasing $H_2C{=}O$.[21] The negative charge on the 8-carbon of the produced anion **i5** is stabilized by delocalization across the phenolic end group. The involvement of the 7- and 9-hydroxyl groups in the CID-induced 48 Da loss was verified by MS^2 analysis of model compounds of which the aliphatic end group lacked the propenol side chain (Figure 4 of the Supporting Information). This neutral loss was observed only in those model compounds that bear both a 7- and 9-hydroxyl group (Figure 4A,B of the Supporting Information), but not in the model compounds in which the 9-hydroxy function is absent (Figure 4C,D of the Supporting Information). However, as this fragmentation proceeds easier for *threo*- than for *erythro*-β-aryl ethers,[9] the relative configuration is important, suggesting that the reaction preferentially occurs by a concerted mechanism involving a six-center cyclic transition state. From analysis of the MS^2 spectra of trimers,[26] this combined loss of water and formaldehyde was also observed to occur via charge-remote mechanisms.

(iv) B^- First Product Ion. Cleavage of the 8−O-4′ bond occurs both with charge migration and charge retention, affording the B^- and A^- first product ions, respectively (Figure 2D,E of the Supporting Information). In the case of charge migration leading to the B^- first product ion **i8** (Figure 2D of the Supporting Information, pathway 1), quinone methide conversion of precursor ion **i1** eliminates the 7-hydroxy function that displaces, via a -OH−**i6** anion−neutral complex, the aliphatic end group from the 8-position of **i6** with the simultaneous loss of the phenolic end group as a neutral. Evidence of the structure of B^- ion **i8** is given by its MS^3 spectrum (Figure 1 of the Supporting Information, MS^3 179). MS^3 fragmentation proceeds by water loss and/or methyl radical ($CH_3^{\bullet}$, 15 Da) loss; both are characteristic for the fragmentation of monolignols. The B^- ion-derived MS^3 spectrum is not completely identical to the MS^2 spectra of the monolignols. Clearly, the internal energy of the MS^2-produced B^- ion differs from that of a monolignol that is ionized in the API source.

In an alternative fragmentation pathway (Figure 2D of the Supporting Information, pathway 2), B^- anion **i8** could arise when, upon formation of **i2**, the 9-alkoxide ion attacks the 8-position yielding a neutral epoxide **i9** and B^- anion **i8**. MS^2-

(27) Taylor, L. C. E.; Johnson, R. L.; St. John-Williams, L.; Johnson, T.; Chang, S. Y. *Rapid Commun. Mass Spectrom.* **1994**, *8*, 265–273.

Table 2. MS² First Product Ions and Intensities of Dilignols[a]

(A) 8−O-4′ Linkage

	Loss (Da)	G(*t*8−O-4)G	S(*t*8−O-4)G	G(*t*8−O-4)S	S(8−O-4)S′	G(8−O-4)G′	G(8−O-4)5H	S(8−O-4)5H	G(8−O-4)5H′
Collision energy (%)		35	35	30	35	35	30	30	30
$[M - H^+]^-$		375(0)	405(0)	405(2)	433(0)	373(0)	373(4)	403(0)	371(3)
$[M - H^+ - CH_3^\bullet]^{-\bullet}$	15				418(8)	388(10)			
$[M - H^+ - H_2O]^-$	18	357(2)	*c*	387(6)			355(36)	385(12)	353(14)
$[M - H^+ - CH_2O]^-$	30	*c*	375(1)	375(1)	403(72)	373(80)	343(22)	373(6)	341(8)
$[M - H^+ - H_2O - CH_2O]^-$	48	327(100)	357(100)	357(100)	385(8)	355(5)			
$[M - H^+ - 2CH_2O]^-$	60				373(100)	343(100)			
A^-	*b*	195(24)	225(19)	195(75)			179(100)	209(100)	179(32)
$[A - CH_3^\bullet]^{-\bullet}$	*b*						164(4)	194(22)	
$[A - H_2O]^-$	*b*						161(4)		
$[A - CH_2O]^-$	*b*	165(7)	195(6)	165(26)					
$[B + 2H]^-$	*b*						195(10)		193(44)
B^-	*b*	179(5)	179(2)	209(75)			193(36)	193(23)	191(9)
$B^{-\bullet}$	*b*								192(100)
$[B^\bullet - CH_3^\bullet]^-$	*b*								177(8)

(B) 8−5′ Linkage

	Loss (Da)	H(8−5)H	G(8−5)G	S(8−5)G	S(8−5)G	G(8−5)G′	G(8−5)FA	DDDC	IDDDC
Collision energy (%)		35	30	25	35	30	30	35	35
$[M - H^+]^-$		297(0)	357(4)	387(100)	387(2)	355(1)	371(14)	359(0)	359(0)
$[M - H^+ - H_2O]^-$	18	279(100)	339(100)	369(60)	369(100)	337(31)	353(100)	341(2)	341(100)
$[M - H^+ - CO]^-$	28							331(1)	
$[M - H^+ - CH_2O]^-$	30	267(20)	327(17)	357(13)	357(24)	325(29)	341(39)		329(53)
$[M - H^+ - CO_2]^-$	44						327(33)		
$^{1,2}B^-$	*b*	191(17)	221(26)	221(14)	221(54)	219(100)	235(9)	223(100)	
$[M - H^+ - H_2O - {}^{1,2}A]^-$	*b*	173(5)	203(16)	203(5)	203(23)				
$[M - H^+ - CH_2O - {}^{1,2}A]^-$	*b*	161(3)	191(5)	191(1)	191(11)				
$^0A^-$	*b*		123(1)	153(1)	153(7)				
$[{}^{1,2}B - CH_3^\bullet]^{-\bullet}$	*b*					204(9)		208(1)	
$[{}^{1,2}B - HCO^\bullet]^{-\bullet}$	*b*					190(5)			
$[{}^{1,2}B - CH_3^\bullet - CO]^{-\bullet}$	*b*					176(3)		180(2)	
$[M - H^+ - CO_2 - {}^{1,2}A]^-$	*b*						191(29)		

(C) 8−8′ Linkage

	Loss (Da)	H(8−8)H	G(8−8)G	S(8−8)S	G(8−8)FA	FA(8−8)FA	lariciresinol	secoisolariciresinol
Collision energy (%)		35	35	30	30	30	35	35
$[M - H^+]^-$		297(0)	357(2)	417(12)	371(0)	385(0)	359(0)	361(0)
$[M - H^+ - CH_3^\bullet]^{-\bullet}$	15		342(14)	402(43)			344(54)	346(100)
$[M - H^+ - CH_4]^-$	16						343(7)	
$[M - H^+ - H_2O]^-$	18						341(15)	343(14)
$[M - H^+ - CH_2O]^-$	30	267(5)	327(34)	387(5)			329(100)	331(14)
$[M - H^+ - CO_2]^-$	44				327(100)	341(44)		
$[M - H^+ - CH_2O - CH_3^\bullet]^{-\bullet}$	45						314(9)	
$[M - H^+ - HCOOH]^-$	46	251(17)	311(15)	371(10)				315(8)
$[M - H^+ - CH_2O - H_2O]^-$	48							313(29)
$[M - H^+ - 2CO_2]^-$	88					297(100)		
$^{2,5}X^-$	*b*	121(100)	151(100)	181(100)	151(3)			
$[{}^{2,5}X - CH_3^\bullet]^{-\bullet}$	*b*		136(23)	166(34)	136(1)			
$[{}^{2,5}X - 2CH_3^\bullet]^-$	*b*			151(11)				
$^{1,5,2',4'}X^-$	*b*	145(1)	175(4)	205(6)	175(1)			
$^{1',5',2,4}X'^-$	*b*	145(1)	175(4)	205(6)	189(1)			
$^{1,2}X'^-$	*b*				*c*			

[a] Structures of the compounds are shown in Figure 12 of the Supporting Information. The relative intensity of the first product ions as compared to the base peak is given in parentheses. A and B, and X and X′, refer to the units that carry the charge after fragmentation of the 8−O-4′ or 8−5′ bonding structure, and the 8−8′ bonding structure, respectively. The numbers in superscript prior to A, B, X, or X′ refer to the bonds in the phenylcoumaran or resinol bonding structure that need to fragment to produce the first product ion (see Figures 2 and 3). [b] The neutral loss of this fragmentation depends on the mass of the involved units. [c] The abundance of the first product ion is <1% of the base peak. DDDC, dihydrodehydrodiconiferyl alcohol; IDDDC, isodihydrodehydrodiconiferyl alcohol. The MS² spectrum of DDDC showed also small first product ions at *m/z* 235(1) and 195(2). The MS² spectrum of secoisolariciresinol showed also first product ions at *m/z* 298(11), 223(5), 179(26), 165(45), 147(5), and 122(10).

driven epoxide formation occurs in the Payne rearrangement[28] where the reaction is driven by the ring opening of a preexisting epoxide. Epoxide formation in the gas phase has also been described during the fragmentation of the α-anomer of methyl 3-*O*-benzyl-2,6-dideoxy-D-arabinose.[29] The latter reaction was driven by the loss of methanol. However, the epoxide-generating fragmentation pathway toward B^- ion **i8** is less important because the B^- ion is not observed at all in the MS² spectrum of the 9-hydroxy function-bearing model compound shown in

(28) Dua, S.; Bowie, J. H.; Taylor, M. S.; Buntine, M. A. *Int. J. Mass Spectrom. Ion Processes* **1997**, *165/166*, 139–153.

(29) Binkley, R. W.; Binkley, E. R.; Duan, S.; Tevesz, M. J. S.; Winnik, W. *J. Carbohydr. Chem.* **1996**, *15*, 879–895.

Table 3. FT-ICR-MS Data[a]

	m/z	Empirical formula	Δppm	Loss
G(*t*8−O-4)**G**				
$[\underline{M - H^+}]^-$	375.14504	$C_{20}H_{23}O_7$	0.302	H^+
$[\underline{M - H^+} - H_2O]^-$	357.13370	$C_{20}H_{21}O_6$	−1.854	H_2O
$[\underline{M - H^+} - CH_2O]^-$	345.13308	$C_{19}H_{21}O_6$	−3.715[b]	CH_2O
$[\underline{M - H^+} - H_2O - CH_2O]^-$	327.12308	$C_{19}H_{19}O_5$	−2.193	CH_4O_2
A^-	195.06616	$C_{10}H_{11}O_4$	−0.627	$C_{10}H_{12}O_3$
$[A - CH_2O]^-$	165.05569	$C_9H_9O_3$	−0.168	$C_{11}H_{14}O_4$
B^-	179.07127	$C_{10}H_{11}O_3$	−0.546	$C_{10}H_{12}O_4$
G(8−O-4)**5H**				
$[\underline{M - H^+}]^-$	373.12945	$C_{20}H_{21}O_7$	0.465	H^+
$[\underline{M - H^+} - H_2O]^-$	355.11795	$C_{20}H_{19}O_6$	−2.146	H_2O
$[\underline{M - H^+} - CH_2O]^-$	343.11799	$C_{19}H_{19}O_6$	−2.104	CH_2O
A^-	179.07121	$C_{10}H_{11}O_3$	−0.881	$C_{10}H_{10}O_4$
$[A - CH_3^\bullet]^{-\bullet}$	164.04778	$C_9H_8O_3$	−0.686	$C_{11}H_{13}O_4$
$[A - H_2O]^-$	161.06068	$C_{10}H_9O_2$	−0.764	$C_{10}H_{12}O_5$
$[B + 2H]^-$	195.06612	$C_{10}H_{11}O_4$	−0.832	$C_{10}H_{10}O_3$
B^-	193.05047	$C_{10}H_9O_4$	−0.841	$C_{10}H_{12}O_3$
G(8−5)**G**				
$[\underline{M - H^+}]^-$	357.13455	$C_{20}H_{21}O_6$	0.526	H^+
$[\underline{M - H^+} - H_2O]^-$	339.12307	$C_{20}H_{19}O_5$	−2.145	H_2O
$[\underline{M - H^+} - CH_2O]^-$	327.12321	$C_{19}H_{19}O_5$	−1.795	CH_2O
$^{1,2}B^-$	221.08172	$C_{12}H_{13}O_4$	−0.961	$C_8H_8O_2$
$[\underline{M - H^+} - H_2O - {}^{1,2}A]^-$	203.07119	$C_{12}H_{11}O_3$	−0.875	$C_8H_{10}O_3$
$[\underline{M - H^+} - CH_2O - {}^{1,2}A]^-$	191.07121	$C_{11}H_{11}O_3$	−0.825	$C_9H_{10}O_3$
S(8−8)**S**[c]				
$[\underline{M - H^+}]^-$	417.15540	$C_{22}H_{25}O_8$	−0.219	H^+
$[\underline{M - H^+} - CH_3^\bullet]^\bullet$	402.13105	$C_{21}H_{22}O_8$	−2.403	CH_3
$[\underline{M - H^+} - CH_2O]^-$	387.14406	$C_{21}H_{23}O_7$	−2.239	CH_2O
$[\underline{M - H^+} - HCOOH]^-$	371.14925	$C_{21}H_{23}O_6$	−2.053	CH_2O_2
$^{1,5,2',4'}X^-$	205.08683	$C_{12}H_{13}O_3$	−0.916	$C_{10}H_{12}O_5$
$^{2,5}X^-$	181.05046	$C_9H_9O_4$	−0.952	$C_{13}H_{16}O_4$
$[^{2,5}X - CH_3^\bullet]^{-\bullet}$	166.02703	$C_8H_6O_4$	−0.766	$C_{14}H_{19}O_4$

[a] CID was performed in the ion trap using a 35% collision energy, whereas detection occurred in the ion cyclotron. The $[\underline{M - H^+}]^-$ precursor ion was measured using full MS scanning in the ion cyclotron. [b] Deviation partially due to its low abundance. [c] IRMPD fragmentation of the $[\underline{M - H^+} - HCOOH]^-$ first product ion of **S**(8−8)**S** yielded a second product ion at *m/z* 205.08694 ($C_{12}H_{13}O_3$, Δppm = −0.379), i.e., with the same accurate *m/z* value as the $^{1,5,2',4'}X^-$ first product ion (the FT-MS measurement of the CID-generated second product ions was not sensitive enough in the lower *m/z* range; hence, IRMPD fragmentation in the ion cyclotron was used). In addition, direct infusion MS^n analysis using the ion trap showed that the MS^4 spectrum of the CID-generated second product ion [*m/z* 190 (100%), 175 (50%)] was similar to the MS^3 spectrum of the $^{1,5,2',4'}X^-$ first product ion [*m/z* 190 (100%), 175 (46%)].

Figure 4B of the Supporting Information, but clearly present in that of the model compound that lacks a 9-hydroxy function (Figure 4D of the Supporting Information).

(v) A^- and $[A - CH_2O]^-$ First Product Ions. A charge-driven fragmentation pathway for A^- anion **i11** can only be proposed assuming the temporary existence of a neutral−B^- anion complex (Figure 2E of the Supporting Information): when the 7-hydroxy group displaces the aliphatic end group from the 8-position of **i6**, the initially formed B^- ion **i8** abstracts a proton from the phenolic end group-derived neutral **i7**, yielding the A^- first product ion **i11**. Clearly, the 9-hydroxy function does not take part in the dissociation step as the A^- ion is also the base peak in the model compounds displayed in Figure 4C,D of the Supporting Information, each of which lacks a 9-hydroxy function. Nevertheless, formation of A^- ion **i11** preferentially occurs via removal of a proton from the 9-hydroxy function in the **i7**−**i8** neutral−anion complex because MS^3 dissociation of A^- ion **i11** proceeds by formaldehyde loss (Figure 1 of the Supporting Information, MS^3 195) and the $[A - CH_2O]^-$ first product ion **i12** appears in the MS^2 spectrum of the model compound that bears a 9-hydroxy group (Figure 4B of the Supporting Information), but is not observed in the MS^2 spectra of the model compounds shown in Figure 4C,D of the Supporting Information.

If a charge-remote fragmentation is envisaged for A^- ion formation (Figure 2E of the Supporting Information, alternative pathway 1), the 8−O-4′ ether function might abstract the acidic 7-proton with the consequent formation of a 7−8 double bond and the loss of the aliphatic end group, yielding the **i13** ion. Such a charge-remote fragmentation is evident from fragmentation studies with trilignols.[26]

Although less likely, an alternative fragmentation mechanism producing the A^- ion (Figure 2E of the Supporting Information, alternative pathway 2) could involve a solvent molecule. Such an E1-like reaction mechanism via a complex-bound water molecule has been previously reported to occur in an ion trap.[30] Here, the water molecule protonates the ether group, which then clips off from the 8-carbon, providing ion **i14**. The resulting 8-cation is then neutralized by the formation of a double bond (anion **i13**) following the abstraction of the 7-proton by the complex-bound hydroxide ion.

In summary, during CID of β-aryl ethers, the phenoxide−quinone methide conversion of **i1** expels the 7-hydroxy function (Figure 2A), yielding a hydroxide anion−neutral complex. Acting as a base, this hydroxide anion abstracts a proton from the 9-hydroxy group of **i6**, affording the loss of water (−18 Da, **i2**). A further

(30) Grossert, J. S.; Fancy, P. D.; White, R. L. *Can. J. Chem.* **2005**, *83*, 1878–1890.

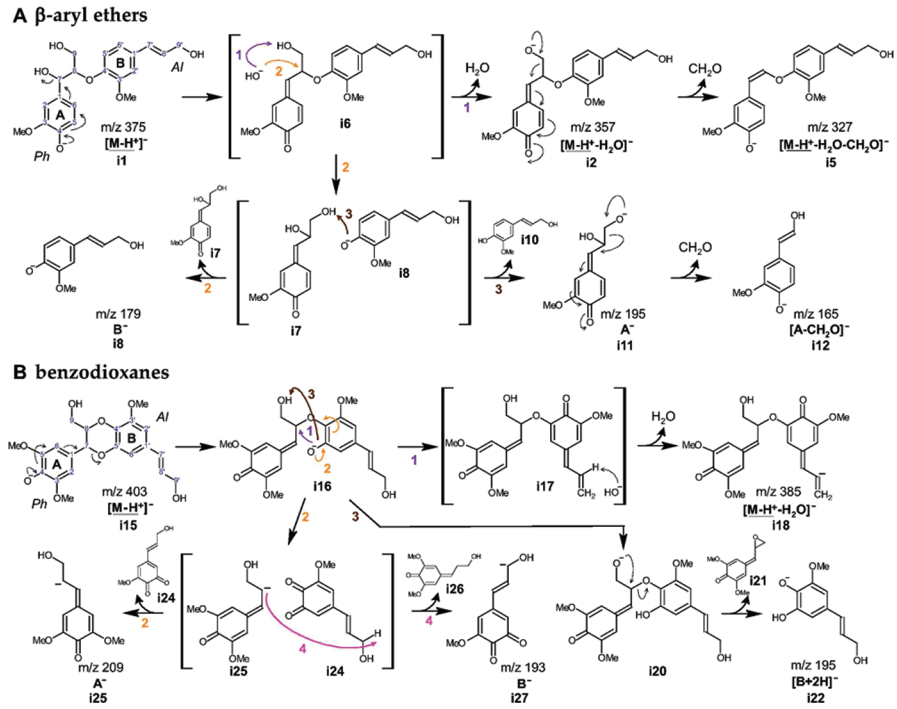

Figure 2. Charge-driven collision-induced dissociation pathways of β-aryl ethers and benzodioxanes. Blue numbers refer to the carbon position, whereas purple, orange, brown, and magenta numbers indicate the different fragmentation pathways. Each intermediate is annotated by **i** followed by a unique number in boldface. The naming convention for the first product ions is mentioned in the footnotes of Table 2. As the $[M - H^+ - CH_2O]^-$ first product ion of benzodioxanes is mainly due to a charge-remote process, its fragmentation pathway is not displayed. Anion−neutral complexes are shown in brackets.

formaldehyde loss (−30 Da, giving a total of −48 Da, **i5**) occurs upon 1,2-elimination. Alternatively, the released 7-hydroxy group nucleophilically attacks the 8-position with the formation of B^- ion **i8**. A^- ion **i11** is then produced by the complex-mediated abstraction of the proton from the 9-hydroxy function of **i7** by B^- ion **i8**.

MS^2 Spectra of Benzodioxanes. Small neutral losses of 18 and 30 Da (see Table 2A), corresponding to the $[M - H^+ - H_2O]^-$ and $[M - H^+ - CH_2O]^-$ first product ions, respectively, and bonding structure cleavages yielding the A^-, B^-, $[A - CH_3^{\bullet}]^{-\bullet}$, $[A - H_2O]^-$, and $[B + 2H]^-$ are observed in the MS^2 spectra of monolignol-derived benzodioxanes (Figure 2B and Figures 5 and 6 of the Supporting Information).

(i) $[M - H^+ - H_2O]^-$ First Product Ion. Only one charge-driven dissociation pathway for the water loss (Figure 6A of the Supporting Information) can be envisioned in which the $[M - H^+ - H_2O]^-$ first product ion would afford second product ions at *m/z* 175 and 209 as observed in the MS^3 spectrum of this first product ion of **S**(8−O-4)**5H** (Figure 5 of the Supporting Information, MS^3 385). Water loss is initiated by a phenoxide−quinone methide conversion of precursor ion **i15** involving cleavage of the 7−O-5′ bond. The new aliphatic end group-associated 5′-phenoxide anion of **i16** then attacks the 8-position with the subsequent cleavage of the 8−O-4′ bond and the formation of an 8−O-5′ bond. The aliphatic end group will be subjected to a phenoxide−quinone methide conversion, leading to the loss of the 9′-hydroxyl group. Subsequently, the resulting hydroxide anion abstracts the C8′ proton via an $^-$OH−**i17** anion−neutral complex. Further CID of the $[M - H^+ - H_2O]^-$ first product ion **i18** would cleave the 8−O-5′ bond, yielding a second product ion associated with the phenolic end group at *m/z* 209 and, following a neutral−anion complex-mediated proton abstraction, a second product ion associated with the aliphatic end group at *m/z* 175 (Figure 5 of the Supporting Information, MS^3 385).

(ii) $[M - H^+ - CH_2O]^-$ and $[B + 2H]^-$ First Product Ions. Charge-driven formaldehyde loss (Figure 6B of the Supporting Information) also proceeds via the formation of an aliphatic end group phenoxide anion **i16**. In this case, following the abstraction of the 9-OH proton by the 5′-phenoxide anion, formaldehyde is expelled from **i20**, yielding anion **i23**. During MS^3 fragmentation of this $[M - H^+ - CH_2O]^-$ first product ion of **S**(8−O-4)**5H** (Figure 5 of the Supporting Information, MS^3 373), a proton transfer from the 5′-O-position to the 8-position via a six-center intermediate leads to a rearrangement in which the aliphatic end group is expelled as an *o*-quinone neutral. This rearrangement yields the ions at *m/z* 179 and 193 (Figure 5 of the Supporting Information, MS^3 373). In addition to these second product ions, a base peak at *m/z* 209 is observed in the MS^3 spectrum. MS^4 fragmentation indicates that this ion represents a sinapyl alcohol moiety (Figure 5 of the Supporting Information, MS^4 209). Therefore, formaldehyde loss upon CID of **S**(8−O-4)**5H** does not solely occur from the syringyl unit, yielding **i23**, but is even more easily expelled from the aliphatic end group by a charge-remote mechanism yielding the **i19** anion (Figure 6B of the Supporting Information). In addition, the 9-alkoxide anion from **i20** may attack the 8-position, cleaving the 8−O-4′ bond and yielding the neutral phenolic end group-associated epoxide **i21** and the $[B + 2H]^-$ ion **i22** (Figure 6B of the Supporting Information). $[B + 2H]^-$ ion **i22** represents the 5-hydroxyconiferyl alcohol anion; the MS^3 spectrum of this

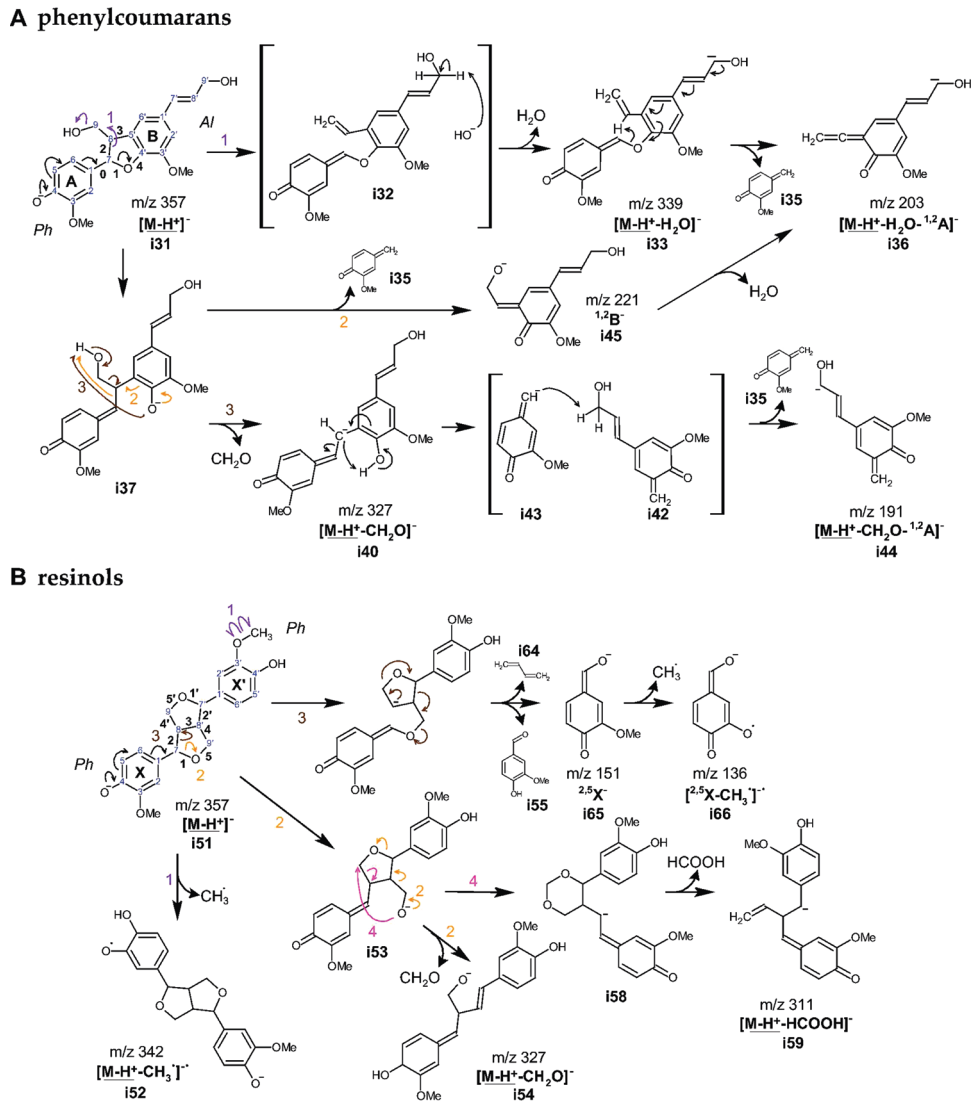

Figure 3. Charge-driven collision-induced dissociation pathways of phenylcoumarans and resinols. Blue numbers refer to the carbon position. Within the bonding structure, each bond is indicated by a black number. Purple, orange, brown, and magenta numbers indicate the different fragmentation pathways. Each intermediate is annotated by **i** followed by a unique number in boldface. The naming convention for the first product ions is mentioned in the footnotes of Table 2. Anion−neutral complexes are shown in brackets.

first product ion (Figure 5 of the Supporting Information, MS^3 195) shows losses of water and/or a methyl radical and is analogous to the MS^2 spectra obtained for monolignols.

(iii) A^- and B^- First Product Ions. The A^- and B^- ions (Figure 6C,D of the Supporting Information) might originate from retro cleavage of the **i16** anion. This retro cleavage leads to a neutral *o*-quinone **i24** representing the aliphatic end group (Figure 6C of the Supporting Information) and the phenolic end group-derived A^- anion **i25**. The latter can lose water or a methyl radical leading to the $[A - H_2O]^-$ and $[A - CH_3]^{-\bullet}$ first product ions (Table 2A) as evidenced from MS^3 fragmentation (Figure 5 of the Supporting Information, MS^3 209). In agreement with the proposed structure for A^- ion **i25**, the MS^3 spectrum was similar to the MS^2 spectrum of sinapyl alcohol (data not shown). When A^- ion **i25** remains in complex with the aliphatic end group-derived neutral **i24**, a proton transfer can occur, yielding B^- ion **i27** representing the aliphatic end group (Figure 6D of the Supporting Information). As **i24** is an *o*-quinone, the transfer of a proton occurs from the acidic 8′-position or from the less acidic 9′-hydroxy group. Therefore, depending on the position of the negative charge, further MS^3 fragmentation of B^- ion **i27** results in the loss of a methyl radical or a formaldehyde (Figure 5 of the Supporting Information, MS^3 193).

(iv) $B^{-\bullet}$ and $[B^{\bullet} - CH_3^{\bullet}]^-$ First Product Ions. In addition to a retro cleavage, a homolytic fission of the 8−O-4′ bond in **i16′** occurs when a cinnamaldehyde-derived aliphatic end group is present (Figure 6E of the Supporting Information), affording $B^{-\bullet}$ ion **i29**. Further methyl radical loss, probably followed by a rearrangement to a more stable *o*-quinone, delivers the $[B^{\bullet} - CH_3^{\bullet}]^-$ first product ion **i30**.

In summary, the charge-driven fragmentations upon CID of benzodioxanes (Figure 2B) proceed via phenoxide−quinone methide conversion of **i15** in which the 7−O-5′ linkage is broken and an aliphatic end group phenoxide anion **i16** is created. As a base, this anion abstracts the 9-OH proton. 9-Alkoxide anion **i20** then attacks the 8-position, leading to $[B + 2H]^-$ ion **i22**. Alternatively, retro cleavage of the aliphatic end group phenoxide ion **i16** yields the A^- **i25** and B^- **i27** ions. Finally, the **i16** anion looses water when the aliphatic end group-associated

5′-phenoxide anion attacks the 8-position, yielding the **i18** product ion. Besides neutral losses of water and formaldehyde, a very weak first product ion was always observed because of the combined loss of water and formaldehyde (−48 Da).

MS² Spectra of Phenylcoumarans. A second linkage that is frequently encountered in dehydrodimers of monolignols is the 8−5′ linkage, yielding phenylcoumaran bonding structures. Upon CID of monolignol-derived phenylcoumarans, water and formaldehyde losses lead to the major first product ions, i.e., the $[\underline{M - H^+} - H_2O]^-$ and $[\underline{M - H^+} - CH_2O]^-$ ions, whereas cleavage of the bonding structure yields the $^{1,2}B^-$, $[\underline{M - H^+} - H_2O - {}^{1,2}A]^-$, and $[\underline{M - H^+} - CH_2O - {}^{1,2}A]^-$ first product ions (Table 2B, Figure 3A, and Figures 7 and 8 of the Supporting Information).

(i) $[\underline{M - H^+} - H_2O]^-$ and $[\underline{M - H^+} - H_2O - {}^{1,2}A]^-$ First Product Ions. A charge-driven hydroxide loss (Figure 8A of the Supporting Information) followed by an anion−neutral-mediated proton transfer with the production of a water molecule can be hypothesized for both aliphatic alcohol groups. A loss of water from the side chain of the phenolic end group would be initiated by a phenoxide−quinone methide conversion of precursor ion **i31** with the concomitant cleavage of the 7−8 bond. The subsequent formation of an 8−9 double bond would then expel the 9-hydroxy group as a hydroxide anion which, via a $^-$OH−**i32** anion−neutral complex, abstracts the acidic C9′ proton of the aliphatic end group leading to anion **i33**. This first product ion could logically further fragment into the $[\underline{M - H^+} - H_2O - {}^{1,2}A]^-$ ion **i36**, which is present in the MS² spectrum and consistent with the MS³ fragmentation of $[\underline{M - H^+} - H_2O]^-$ anion **i33** (Figure 7 of the Supporting Information, MS³ 339). The MS³ spectrum of $[\underline{M - H^+} - H_2O - {}^{1,2}A]^-$ ion **i36** shows methyl radical and/or CO losses (Figure 7 of the Supporting Information, MS³ 203). The $[\underline{M - H^+} - H_2O^+ - {}^{1,2}A]^-$ ion is not formed when the aliphatic end group is derived from a hydroxycinnamaldehyde because its C9′ hydrogen is much less acidic (Table 2B). Alternatively, phenoxide−quinone methide conversion of the phenolic end group might cleave the 7−O-4′ bond, yielding ion **i37** (Figure 8A of the Supporting Information, alternative pathway). A subsequent phenoxide−quinone methide conversion of the aliphatic end group would result in the loss of the 9′-hydroxy group, yielding a water molecule and anion **i39** via a $^-$OH−**i38** anion−neutral complex-mediated proton transfer. However, further MS^n fragmentation (Figure 7 of the Supporting Information, MS³ 339 and MS⁴ 203) of the resulting product ions does not support a substantial contribution of this pathway to the observed water loss (if anion **i39** contributed to the peak intensity of the $[\underline{M - H^+} - H_2O]^-$ first product ion, a water loss would have been expected upon MS³ fragmentation of the ion at m/z 339).

(ii) $[\underline{M - H^+} - CH_2O]^-$ and $[\underline{M - H^+} - CH_2O - {}^{1,2}A]^-$ First Product Ions. 1,2-Elimination of the aliphatic alcohol as formaldehyde[21] (Figure 8B of the Supporting Information) starts when the phenoxide ion from **i37** abstracts the proton from the 9-OH function which is subsequently lost as formaldehyde. C8 carbanion **i40** ($[\underline{M - H^+} - CH_2O]^-$) is resonance-stabilized and will probably attract the phenolic proton of the aliphatic end group by a five-membered cyclic transition state, yielding ion **i41**. Following a phenoxide−*o*-quinone methide conversion of the aliphatic end group from **i41**, the A ring is expelled. While remaining in a complex, the A ring quinone methide anion **i43** abstracts a C9′ proton from the B ring neutral **i42**, yielding the $[\underline{M - H^+} - CH_2O - {}^{1,2}A]^-$ anion **i44**. This pathway was supported by the MS³ fragmentation of the $[\underline{M - H^+} - CH_2O]^-$ **i40** first product ion (Figure 7 of the Supporting Information, MS³ 327), whereas MS² of the $[\underline{M - H^+} - CH_2O - {}^{1,2}A]^-$ ion yields methyl radical and/or CO losses (Figure 7 of the Supporting Information, MS² 191), which is in favor of an *o*-quinone methide structure with the charge located at the 9-position.

(iii) $^{1,2}B^-$ and $[\underline{M - H^+} - H_2O - {}^{1,2}A]^-$ First Product Ions. The phenylcoumaran bonding structure of **i37** can also be retro cleaved (Figure 8C of the Supporting Information). The resulting $^{1,2}B^-$ ion **i45** is hereby likely formed in a concerted reaction, in which, upon phenoxide−*o*-quinone methide conversion of the aliphatic end group of **i37**, the breakage of the 7−8 bond occurs concomitantly with the abstraction of the 9-OH proton by the A ring quinone methide moiety. The resulting $^{1,2}B^-$ alkoxide ion **i45** would dissociate further by the loss of water rather than formaldehyde. This is indeed observed in the MS³ spectrum (Figure 7 of the Supporting Information, MS³ 221). Water loss would contribute to the peak intensity of the $[\underline{M - H^+} - H_2O - {}^{1,2}A]^-$ ion **i36** which is verified by MS⁴ (Figure 7 of the Supporting Information, MS⁴ 203). Further support for this retro cleavage mechanism is obtained from the MS² spectra of isodihydrodehydrodiconiferyl alcohol (IDDDC, Table 2B, Figure 12 of the Supporting Information). The reduced phenylcoumaran bonding structure of IDDDC prohibits the formation of a $^{1,2}B^-$ ion. When the aliphatic end group is derived from a cinnamaldehyde or a dihydrocinnamyl alcohol [e.g., dihydrodehydrodiconiferyl alcohol (DDDC); Figure 12 of the Supporting Information], the retro cleavage leading to the $^{1,2}B^-$ ion is much more pronounced (Table 2B), and its further dissociation by the loss of a HCO radical or a methyl radical and/or the combined loss of CO and/or a methyl radical is visible in the MS² spectrum (Figure 8D of the Supporting Information).

In the case of a cinnamic acid aliphatic end group, the charge is localized on the acid function, making dehydration and decarboxylation major fragmentation pathways (Table 2B).[21] The retro cleavage leading to the $^{1,2}B^-$ ion is more suppressed because of the charge localization on the acid group. Here, the $^{1,2}B^-$ ion might arise from a charge-remote mechanism. However, a combined decarboxylation/retro cleavage yields still a major $[\underline{M - H^+} - CO_2 - {}^{1,2}A]^-$ first product ion (Table 2B).

In summary, the phenoxide anion−quinone methide conversion of the phenolic end group of phenylcoumarans leads to the B ring phenoxide anion **i37** (Figure 3A), which yields $^{1,2}B^-$ anion **i45** via a retro cleavage or affords a formaldehyde loss (**i40** ion) when the B ring phenoxide anion abstracts the 9-OH proton of the phenolic end group. Further conversion of the aliphatic end group to an *o*-quinone methide explains $[\underline{M - H^+} - CH_2O - {}^{1,2}A]^-$ anion **i44**. Phenoxide anion−quinone methide conversion of the A ring might also break the 7−8 bond with the concomitant elimination of the 9-OH group (**i32**). Abstraction of the aliphatic end group C9′ proton by this hydroxide anion results in water loss (**i33**). Subsequent retro

cleavage produces $[M - H - H_2O - {}^{1,2}A]^-$ anion **i36**. The latter ion is also formed by the loss of water from $^{1,2}B^-$ ion **i45**.

MS^2 Spectra of Resinols. A third linkage that occurs after dimerization of monolignol radicals is the 8−8′ linkage in so-called resinol structures. As radical coupling at the 8-position is favored, the 8−8′ linkage is predominant in monolignol dehydrodimer mixtures, particularly with sinapyl alcohol. The $[\underline{M - H^+} - CH_3^\bullet]^{-\bullet}$, $[\underline{M - H^+} - CH_2O]^-$, and $[\underline{M - H^+} - HCOOH]^-$ first product ions due to methyl radical, formaldehyde, and formic acid (HCOOH, −46 Da) loss, respectively, are visible in the MS^2 spectra of monolignol-derived resinols. Furthermore, bonding structure cleavages lead to the $^{2,5}X^-$, $[^{2,5}X - CH_3^\bullet]^{-\bullet}$, and $^{1,5,2',4'}X^-$ first product ions (Table 2C, Figure 3B, and Figures 9 and 10 of the Supporting Information).

(i) $[\underline{M - H^+} - CH_3^\bullet]^{-\bullet}$ First Product Ion. The absence of aliphatic alcohol, aldehyde, or acid functions in resinol structures allows the loss of methyl radical from methoxyl groups to become more prevalent (Figure 10A of the Supporting Information). This neutral loss was not observed for **H**(8−8)**H** as this dilignol does not contain methoxyl groups. The loss of a neutral alkyl radical from alkyl aryl ether negative ions by homolytic fission is a well-known favorable fragmentation reaction in the gas phase.[31]

(ii) $[\underline{M - H^+} - CH_2O]^-$ First Product Ion. As also observed for β-aryl ethers, benzodioxanes, and phenylcoumarans, a formaldehyde loss occurs upon CID of resinols (Figure 10B of the Supporting Information). According to a charge-driven mechanism, this involves again a phenoxide−quinone methide conversion in which the 7−O-9′ ether bond from precursor ion **i51** is broken. The resulting 9′-O-alkoxide anion **i53** will then be subjected to a 1,2-elimination, yielding $[\underline{M - H^+} - CH_2O]^-$ ion **i54**.[21] In the case of units derived from ferulic acid, the main fragmentation pathway is decarboxylation (Table 2C). This $[\underline{M - H^+} - CO_2]^-$ first product ion is formed following a fragmentation pathway similar to that used during formaldehyde loss.

(iii) $^{1,5,2',4'}X^-/^{1',5',2,4}X'^-$ First Product Ion. The formation of the $^{1,5,2',4'}X^-/^{1',5',2,4}X'^-$ anion (Figure 10C of the Supporting Information) occurs when the 9′-oxyanion from **i53** attacks the 9-position, yielding a vanillin neutral loss (**i55**). The remaining tetrahydrofuran carbanion **i56** rearranges, affording a formaldehyde loss and the resonance-stabilized C8 carbanion $^{1,5,2',4'}X^-$ (**i57**). This whole reaction mechanism implies that the 9′-oxyanion acts as a nucleophile rather than as a base, whereas the reverse is true in the gas phase.[32] However, the two most acidic positions on the resinol structure are the α-protons to the phenol or quinone groups, and it is not possible to deduce the formation of the $^{1,5,2',4'}X^-/^{1',5',2,4}X'^-$ anion following the abstraction of one of these protons by the 9′-oxyanion.

(iv) $[\underline{M - H^+} - HCOOH]^-$ First Product Ion. In MS^2 spectra of resinols, a first product ion attributable to a 46 Da loss was observed (Figure 10C of the Supporting Information), that, on the basis of accurate data obtained by FT-MS (Table 3), corresponds to a CH_2O_2 loss. Even at a lower collision energy, no *m/z* first product ions due to H_2O, CO, CO_2, or H_2 loss are formed, indicating that the 46 Da loss is in agreement with the elimination of formic acid. Furthermore, IRMPD of the CID-generated $[\underline{M - H^+} - HCOOH]^-$ first product ion of **S**(8−8)**S** yielded a second product ion (*m/z* 205.08694) with the same accurate mass (in Table 3, see the footnotes; see also the CID-generated MS^3 spectrum of the ion at *m/z* 311 in Figure 9 of the Supporting Information showing the analogous **G**-associated second product ion at *m/z* 175) as the $^{1,5,2',4'}X^-/^{1',5',2,4}X'^-$ first product ion. In addition, the CID-generated MS^4 spectrum of this second product ion was analogous to the MS^3 spectrum of the $^{1,5,2',4'}X^-/^{1',5',2,4}X'^-$ anion (data not shown). Therefore, a plausible charge-driven fragmentation pathway involves the rearrangement of resinol structure **i51** into 1,3-dioxane structure **i58**, from which HCOOH loss would more easily occur affording the **i59** anion. A further cleavage of the 7−8 bond followed by an **i60**−**i61** anion−neutral complex-mediated proton transfer would then lead to the **i63** anion and a quinone methide neutral loss (see the Results and Discussion of the Supporting Information for a more detailed description).

(v) $^{2,5}X^-$ and $[^{2,5}X - CH_3^\bullet]^{-\bullet}$ First Product Ions. The rearrangement of phenoxide anion **i51** into a quinone methide might invoke a retro cleavage of the resinol ring with the formation of 1,3-butadiene (**i64**) and vanillin (**i55**) as neutrals (Figure 10D of the Supporting Information). This retro cleavage leads to the prominent $^{2,5}X^-$ first product ion **i65**, which might subsequently loose a methyl radical affording the **i66** ion as supported by MS^3 (Figure 9 of the Supporting Information, MS^3 151). The postulated reaction mechanisms that yield the $^{2,5}X^-$ and $^{1,5,2',4'}X^-/^{1',5',2,4}X'^-$ anions necessitate the presence of an intact resinol bonding structure, which is supported by the absence of these anions in the MS^2 spectra of lariciresinol and secoisolariciresinol (Table 2C and Figure 12 of the Supporting Information).

In summary, the MS^2 spectra of resinols revealed methyl radical loss due to a homolytic cleavage (−15 Da, Figure 3B). In addition, a phenoxide anion−quinone methide conversion initiated multiple fragmentations. On the one hand, cleavage of the 7−8 bond led to a retro cleavage generating 1,3-butadiene (**i64**), a benzaldehyde neutral (**i55**), and $^{2,5}X^-$ ion **i66**. On the other hand, cleavage of the 7−O-9′ bond yielded the $^{1,5,2',4'}X^-/^{1',5',2,4}X'^-$ ion **i57** following a complex series of reactions or resulted in the elimination of HCOOH (**i59**) after a resinol−1,3-dioxane rearrangement, further of which fragmentation also contributed to the $^{1,5,2',4'}X^-/^{1',5',2,4}X'^-$ ion intensity.

CONCLUSIONS

Lignomics comprises the profiling of all phenolics, such as phenylpropanoids, lignans, and lignin oligomers, for which the biosynthesis and/or regulation is connected with lignin biosynthesis. As for metabolomics in general, the major bottleneck in lignomics is the identification of unknowns. Except for small phenolics and phenylpropanoids, information about their CID spectra is still scarce. To allow a more efficient structural elucidation by MS, we have elucidated the fragmentation pathways in the gas phase of the major bonding structures. In the absence of a carboxylic acid function, small neutral losses are observed that are typical for each bonding structure. The spectra of both β-aryl ethers and benzodioxanes are recognized by losses of 18 Da (water), 30 Da (formaldehyde), and 48 Da (water/formaldehyde). However, the first product ion corresponding to the 48 Da loss is a major peak in the spectra of β-aryl ethers, but hardly visible in those of benzodioxanes. Major first

(31) Bowie, J. H. *Mass Spectrom. Rev.* **1984**, *3*, 161–207.
(32) Harrison, A. G. *Chemical Ionization Mass Spectrometry*, 2nd ed.; CRC Press: Boca Raton, FL, 1992.

product ions due to losses of 18 and 30 Da are observed for phenylcoumarans. In addition to a 30 Da loss, resinols show peaks corresponding to the loss of a methyl radical (15 Da, only when the units are methoxylated) and of formic acid (46 Da). Following the characterization of the bonding structure, the aromatic units involved in this dimer might then be deduced from the molecular mass and from fragmentations that break the bonding structure. Additionally, whenever a substituent is present, the latter fragmentations enable us to pinpoint the aromatic unit on which it is localized. Among the more prominent of these fragmentations are the A^- and B^- ions for the β-aryl ethers and the benzodioxanes, the $^{1,2}B^-$ ion for the phenylcoumarans, and the $^{2,5}X^-$ ions for the resinols. The same CID-based identification approach, i.e., classification of the compound (such as a flavanone, flavone, flavonol, etc.) followed by annotation of the aromatic units and their substituents, has already been firmly established for the flavonoids.[23,33,34]

These fragmentations allow annotation of both the bonding structure and the aromatic units involved. Therefore, this work laid the foundation for the development of an MS-based sequencing algorithm that allowed the identification of 36 oligolignols present in poplar xylem.[26] These oligolignols probably belonged to the methanol-extractable lignin oligomer fraction in the cell wall, but the possibility that some of them were sesqui- or dineolignans cannot be excluded.

(33) Ma, Y. L.; Li, Q. M.; Van den Heuvel, H.; Claeys, M. *Rapid Commun. Mass Spectrom.* **1997**, *11*, 1357–1364.
(34) Fabre, N.; Rustan, I.; de Hoffmann, E.; Quetin-Leclercq, J. *J. Am. Soc. Mass Spectrom.* **2001**, *12*, 707–715.

ACKNOWLEDGMENT

The authors thank Paul Schatz (US Dairy Forage Research Center, USDA-Agricultural Research Service, Madison, WI) for the synthesis of S-propan-1-ol and S-propan-2-ol and Tsutomu Ishikawa (Chiba University, Chiba, Japan) for providing nitidanin. This work was supported by grants from the Research Foundation-Flanders (Grants G.0352.05N and G.0637.07), by the Stanford University Global Climate and Energy Project (Towards New Degradable Lignin Types), by the Multidisciplinary Research Project "Biotechnology for a sustainable economy" of Ghent University, and the "Bijzondere Onderzoeksfonds-Zware Apparatuur" of Ghent University for the FTICR-MS instrument (Grant 174PZA05). H.K., F.L., and J.R. were funded in part by the DOE Great Lakes Bioenergy Research Center (DOE Office of Science BER DE-FC02-07ER64494).

NOTE ADDED AFTER ASAP PUBLICATION

This paper was published on the Web on August 26, 2010, with a minor text error in footnote b of Table 3 and an additional grant number added in the Acknowledgment paragraph. The corrected version was reposted on September 3, 2010.

SUPPORTING INFORMATION AVAILABLE

Additional information as noted in the text. This material is available free of charge via the Internet at http://pubs.acs.org.

Received for review April 13, 2010. Accepted August 10, 2010.

AC100968G